

Robust tracking for nanopositioning stages using sliding mode control with active disturbance rejection: Design and implementation

Journal of Vibration and Control
2023, Vol. 29(15-16) 3809–3822
© The Author(s) 2022
Article reuse guidelines:
sagepub.com/journals-permissions
DOI: 10.1177/10775463221106016
journals.sagepub.com/home/jvc


Guangwei Wang¹, Bo Wang², Jin Zhao¹, and Meng Tao¹

Abstract

This paper presents the design and implementation of a novel sliding mode control integrated with active disturbance rejection (SMCDR) for precise robust trajectory tracking of piezoelectric nanopositioning stages. The model uncertainties, nonlinearity, and external disturbances of the piezoelectric nanopositioning stage are regarded as a lumped disturbance, which is estimated by an extended state observer. The active disturbance rejection control (ADRC) strategy is used to realize a preliminary trajectory tracking, while the sliding mode control is adopted to handle the estimation error and residual uncertainties, and to improve the tracking performance. The exponential stability of the proposed SMCDR is proved using Lyapunov's direct method. The proposed SMCDR controller combines the strength of both ADRC and sliding mode control, exhibits a simple structure, requires only the position measurements, and does not require any information of model parameters except for an approximate constant gain. Experimental results reveal the robustness of the SMCDR approach in suppressing the hysteresis of piezoelectric actuator, and illustrate the superior performance over conventional ADRC, integral sliding mode controller (ISMC) and PID controller for trajectory tracking control of piezoelectric nanopositioning stages.

Keywords

nanopositioning stage, sliding mode control, active disturbance rejection control, experimental implementation

Introduction

Piezoelectric nanopositioning stages have been intensively utilized in precision engineering applications, such as scanning electron microscopes, biological manipulations, and surgical devices (Lau et al. 2019; Wang and Xu 2017; Xie et al. 2019). Such applications are enabled by the outstanding attributes of piezo-driven motion stages such as fine resolution, quick response, large energy density, and high operation bandwidth, etc. (Ling et al. 2021). However, piezoelectric actuators (PEAs) exhibit intrinsic nonlinear characteristics in the voltage-driven motion, which is mainly caused by the hysteresis effects of the ferroelectric material (Tao et al. 2021). The hysteresis of piezoelectric stages usually exhibits both rate-dependent and amplitude-dependent behaviors, which makes the system modeling and parameter identification extremely difficult (Feng et al. 2019). Furthermore, the effect of external disturbances is another obstacle to the motion control of PEAs. Such weaknesses degrade the performance of trajectory tracking, which hinders the implementations of PEAs in the precision motion control applications.

Various control strategies have been developed in the literature to mitigate the negative effects of hysteresis on the trajectory tracking accuracy (Li et al. 2021; Sabarianand et al. 2020; Yang et al. 2020). These control strategies can be generally divided into two categories: hysteresis-model-based control and hysteresis-model-free control. In the hysteresis-model-based control approaches, a mathematical model will be developed to precisely describe the nonlinear hysteresis effects. Then, its inverse model is adopted to cancel out the hysteresis effects accordingly (Yang et al. 2020). Although such approaches can be realized using feedforward control, and does not require any position

¹School of Mechanical Engineering, Guizhou University, Guiyang, China

²Department of Mechanical Engineering, Villanova University, Villanova, PA, USA

Received: 13 January 2022; revised: 5 April 2022; accepted: 8 May 2022

Corresponding author:

Guangwei Wang, School of Mechanical Engineering, Guizhou University, Guiyang 550025, China.
Email: gwwang@gzu.edu.cn

measurements (Gu et al. 2014), the hysteresis models are highly complicated, and the model parameters can hardly be identified accurately. On the contrary, the hysteresis-model-free approaches consider the hysteresis effects of PEAs as external disturbances of the nominal model. Consequently, feedback controllers are designed to suppress the lumped disturbances and to achieve the precise trajectory tracking (Li et al. 2020; Shahabi et al. 2020). Compared with the hysteresis-model-based strategy, the hysteresis-model-free strategy is of particular significance in many applications due to its simplicity and robustness.

Numerous controllers based on hysteresis-model-based strategy have been proposed to realize precision position tracking for nanopositioning systems (Sabarianand et al. 2020). Li et al. (2016) presented a damping control scheme integrated with recursive delayed position feedback for piezoelectric nanopositioning stages to improve the control bandwidth. A robust adaptive backstepping controller is proposed in Zhang et al. (2017) for piezoelectric systems, in which parametric uncertainties were estimated adaptively while the hysteresis and disturbances are treated as lumped disturbances for elimination. To mitigate the nonlinear effects of hysteresis, Takagi-Sugeno fuzzy logic was adopted to denote hysteresis model and its inverse model was used in designing a fuzzy internal model controller (Li et al. 2015b). Yousef et al. (2019) investigated the precision tracking problem of piezoelectric actuators without hysteresis model based on fuzzy approximation and particle swarm optimization algorithm. Model predictive control was proposed to attenuate the influence of load disturbance, that adopts pole-placement and adaptive techniques to deal with the complicated parameter tuning procedure (Nguyen and Chen 2019).

Among that, sliding mode control (SMC) is one of the most widely studied robust control techniques for piezoelectric stages in the literature (Utkin et al. 2017). Sliding mode control provides the possibility of alleviating the effect of nonlinear dynamics and external disturbances. However, the discontinuous control signal triggers the undesirable chattering phenomenon, which hinders the precision applications of piezo-driven stages. To achieve faster convergence and tackle with chattering problem, terminal SMC (TSMC) was proposed with fractional-order sliding surface (Wu et al. 1998). The singularity problem was further tackled in the nonsingular TSMC (Wang and Xu 2018). In addition, adaptive SMC has been developed to regulate the switching gain of the discontinuous control signal regardless of the upper bound on the uncertain terms. Higher-order SMC (HOSMC) has been proposed to release the restriction of relative degree one for the conventional SMC (Ovalle et al. 2021). However, a complicated control structure is introduced along with the evolution of these algorithms. In particular, accurate platform model or full system state of piezoelectric positioning stage is generally required for constructing

control algorithms to achieve precision tracking performance, which limits their implementation for engineering application.

As an alternative kind of method, active disturbance rejection control (ADRC) has been proposed to alleviate the effects of unexpected disturbances in motion control. The basic idea of ADRC, which was first proposed by Han (Han 1998), is to estimate the model uncertainties and the generalized disturbances by using an extended state observer (ESO). This control scheme is robust to the variation of system dynamics and requires limited model information. Recently, ADRC has been successfully implemented in many practical applications, such as surgical device (Lau et al. 2019), solenoids system (Li et al. 2015a), and vibration suppression (Ramírez-Neria et al. 2021; Xia et al. 2018). Concerning a piezoelectric precision motion stage, the hypothesis of known control gain in ESO is too strict for the piezoelectric hysteresis nonlinearity. To expand the application of ESO, the combination method of sliding mode control method and ESO has been proposed (Alonge et al. 2017; Yao et al. 2021). The parametric uncertainties can be dealt with ESO while its estimation error is compensated by SMC. However, it is still unknown whether such a control scheme is capable of overcoming the parametric uncertainties and strong nonlinearity of the piezo-driven nanopositioning stage. In addition, the proof process of the compound method needs to be improved. Hence, the study is motivated to propose a new controller to attain robust tracking performance for nanopositioning stages while keeping simple structure in design and implementation.

The main contribution of this paper is the design of a novel SMCDR control method, which combines the strength of both SMC and ADRC dedicated to trajectory tracking control of a piezoelectric nanopositioning stage. In particular, the SMCDR offers the advantage of easy implementation, as the ADRC does not require the knowledge of system parameters. Only the knowledge of the control gains is required for the proposed controller. In addition, the presented control method exhibits better performance as compared with the baseline controller while maintaining a simple structure, which is confirmed by a series of experimental results.

The rest of paper is organized as follows. The model description of nanopositioning systems are presented in Section 2. Section 3 presents the SMCDR control design and stability analysis. Experimental setup and implementation of the SMCDR are given in Section 4. Section 5 presents a series of experimental results. Finally, conclusions are provided in Section 6.

System description

The motion of a piezoelectric nanopositioning stage can be modeled as an uncertain second-order nonlinear system

$$\begin{cases} \dot{x}_1 = x_2, \\ \dot{x}_2 = f(x_1, x_2, t) + d(t) + bu(t), \end{cases} \quad (1)$$

where $x_1 \in \mathbb{R}$ and $x_2 \in \mathbb{R}$ represent the position and velocity of the piezoelectric actuator, respectively; $u(t) \in \mathbb{R}$ is the control input; $b > 0$ is an unknown control gain; $f: \mathbb{R} \times \mathbb{R} \times \mathbb{R}_{\geq 0} \rightarrow \mathbb{R}$ represents the nonlinearity of nanopositioning system including the hysteresis effect; $d(t)$ denotes the external disturbances. Note that the gain b and the nonlinearity $f(x_1, x_2, t)$ are unknown. Furthermore, only the position of the piezoelectric actuator x_1 can be measured for feedback purpose.

It is noticed that the unknown nonlinearity and external disturbances can be viewed as a lumped disturbance, that is, $h(t) = f(x_1(t), x_2(t), t) + d(t)$, and by assuming that it is differentiable, the lumped disturbance $h(t)$ can be considered as an augmented state variable x_3 . Hence, the dynamical system (1) can be written into the vector form

$$\begin{aligned} \dot{\mathbf{X}} &= \mathbf{A}\mathbf{X} + \mathbf{B}u(t) + \mathbf{D}\dot{h}(t) \\ y &= \mathbf{C}\mathbf{X} \end{aligned} \quad (2)$$

where

$$\mathbf{A} = \begin{bmatrix} 0 & 1 & 0 \\ 0 & 0 & 1 \\ 0 & 0 & 0 \end{bmatrix}, \mathbf{B} = \begin{bmatrix} 0 \\ b \\ 0 \end{bmatrix}, \mathbf{D} = \begin{bmatrix} 0 \\ 0 \\ 1 \end{bmatrix},$$

$$\mathbf{C} = [1 \quad 0 \quad 0], \mathbf{X} = [x_1 \quad x_2 \quad x_3]^T.$$

Controller design

In this section, the ESO and ADRC controller are first presented to realize preliminary trajectory tracking control. Then, the SMC strategy is integrated with the traditional ADRC to improve the position tracking performance for the piezoelectric nanopositioning stage by compensating for the adverse influence.

Design of extended state observer

In general, position is the only available measurements for piezo-driven nanopositioning stages, which impedes the implementation of controllers requiring full state feedback. To handle this problem, different state observers have been studied in the literature to provide necessary states to control algorithms. A known system model is usually essential for the conventional observer design. However, the hysteresis dynamics of piezoelectric motion stages are complicated and difficult to be modeled. Extended state observers (ESOs) were developed to cope with such a problem (Han 2009). To estimate the state variable, ESO needs only the information of the control input and the position measurements, and correspondingly, the lumped disturbance can

be estimated. Thus, one avoids the usage of velocity measurements and makes it easier to implement control algorithm in practical applications.

The structure of the ESO for system (2) is given by (Guo and Zhao 2011)

$$\begin{aligned} \dot{\hat{x}}_1 &= \hat{x}_2 - \epsilon g_1 \left(\frac{\hat{x}_1 - x_1}{\epsilon^2} \right), \\ \dot{\hat{x}}_2 &= \hat{x}_3 - g_2 \left(\frac{\hat{x}_1 - x_1}{\epsilon^2} \right) + bu, \\ \dot{\hat{x}}_3 &= -\epsilon^{-1} g_3 \left(\frac{\hat{x}_1 - x_1}{\epsilon^2} \right). \end{aligned} \quad (3)$$

The linear extended state observer (LESO) is adopted in this work, that is, functions $g_i(\cdot)$'s are linear for $i = 1, 2, 3$. To facilitate the analysis, define the scaled estimation error as

$$\eta_i = \frac{\tilde{x}_i}{\epsilon^{\rho-i}}, \quad (4)$$

where $i = 1, 2, 3$, $\rho = 3$, ϵ is a positive parameter to be designed, and $\tilde{x}_i = \hat{x}_i - x_i$ is the estimation error. Then, the estimation error system in singularly perturbed form is expressed as

$$\epsilon \dot{\eta} = \mathbf{A}_0 \eta + \epsilon \dot{h} \quad (5)$$

where

$$\begin{aligned} \eta &= [\eta_1 \quad \eta_2 \quad \eta_3]^T, \quad \mathbf{A}_0 = \mathbf{A} - \mathbf{L}\mathbf{C}, \quad \mathbf{e} = [0 \quad 0 \quad -1]^T, \\ \mathbf{L} &= [\beta_1 \quad \beta_2 \quad \beta_3]^T, \quad \epsilon^{2-i} g_i(\tilde{x}_1) = \beta_i \tilde{x}_1, \quad i = 1, 2, 3. \end{aligned}$$

Suppose that the derivative of the lumped disturbance $h(t)$ is bounded, that is, $|\dot{h}(t)| \leq \mathbf{H}$ for all $t \geq 0$. Note that this assumption is reasonable and common in nanopositioning applications. We present the following result.

Theorem 1. Suppose that the matrix \mathbf{A}_0 is Hurwitz. Then, there exist $\epsilon_1^* > 0$ and $T_\gamma > 0$ such that, for every $0 < \epsilon \leq \epsilon_1^*$, the estimation errors satisfy

$$\left| \tilde{x}_i \right| \leq \nu \epsilon^{3-i}, \quad \forall t \geq T_\gamma, \quad i = 1, 2, 3. \quad (6)$$

Proof. Consider the Lyapunov candidate function

$$V(\eta) = \eta^T \mathbf{\Lambda} \eta, \quad (7)$$

where the matrix $\mathbf{\Lambda}$ is the symmetric positive definite solution to the Lyapunov equation $\mathbf{\Lambda} \mathbf{A}_0 + \mathbf{A}_0^T \mathbf{\Lambda} = -\mathbf{Q}$, and \mathbf{Q} is a symmetric positive definite matrix. Differentiating (7) along trajectories of equation (5), we have

$$\begin{aligned}
\dot{V}(\eta) &= 2\eta^T \Lambda \dot{\eta} \\
&= 2\eta^T \Lambda \left(\frac{1}{\epsilon} (\mathbf{A}_0 \eta) + e \dot{h} \right) \\
&= \frac{1}{\epsilon} \eta^T (\Lambda \mathbf{A}_0 + \mathbf{A}_0^T \Lambda) \eta + 2\dot{h} \eta^T \Lambda e \\
&= -\frac{1}{\epsilon} \eta^T \mathbf{Q} \eta + 2\dot{h} \eta^T \Lambda e \\
&= -\frac{W(\eta)}{\epsilon} + 2\dot{h} \eta^T \Lambda e,
\end{aligned} \tag{8}$$

where $\mathbf{W}(\eta) = \eta^T \mathbf{Q} \eta \geq 0$. For functions $V(\boldsymbol{\eta})$ and $W(\boldsymbol{\eta})$, they satisfy

$$\begin{aligned}
\lambda_{\min}(\Lambda) \|\eta\|^2 &\leq V(\eta) \leq \lambda_{\max}(\Lambda) \|\eta\|^2, \\
\lambda_{\min}(\mathbf{Q}) \|\eta\|^2 &\leq W(\eta) \leq \lambda_{\max}(\mathbf{Q}) \|\eta\|^2,
\end{aligned} \tag{9}$$

where $\lambda_{\max}(\cdot)$ and $\lambda_{\min}(\cdot)$ represent the maximal and minimal eigenvalues of matrices, respectively. $\|\cdot\|$ denotes the Euclidean norm of vectors. It follows from equation (9) that

$$\begin{aligned}
\dot{V}(\eta) &\leq -\frac{\lambda_{\min}(\mathbf{Q}) \|\eta\|^2}{\epsilon} + \beta \|\eta\| \\
&\leq -\frac{\lambda_{\min}(\mathbf{Q})}{\epsilon} \frac{V(\eta)}{\lambda_{\max}(\Lambda)} + \beta \frac{\sqrt{V(\eta)}}{\sqrt{\lambda_{\min}(\Lambda)}},
\end{aligned} \tag{10}$$

where $\beta = 2H \|\Lambda e\|$. Next, according to the following identity

$$\overbrace{\sqrt{V(\eta)}} = \frac{\dot{V}(\eta)}{2\sqrt{V(\eta)}}, \tag{11}$$

we obtain

$$\overbrace{\sqrt{V(\eta)}} \leq -\frac{\lambda_{\min}(\mathbf{Q})}{2\epsilon \lambda_{\max}(\Lambda)} \sqrt{V(\eta)} + \frac{\beta}{2\sqrt{\lambda_{\min}(\Lambda)}}. \tag{12}$$

The solution to the above differential inequality can be estimated as (Alonge et al. 2017)

$$\begin{aligned}
\sqrt{V(\eta(t))} &\leq \left(\sqrt{V(\eta(0))} - \frac{\epsilon \beta \lambda_{\max}(\Lambda)}{\sqrt{\lambda_{\min}(\Lambda) \lambda_{\min}(\mathbf{Q})}} \right) \\
&\times e^{-\frac{\lambda_{\min}(\mathbf{Q})}{2\epsilon \lambda_{\max}(\Lambda)} t} + \frac{\epsilon \beta \lambda_{\max}(\Lambda)}{\sqrt{\lambda_{\min}(\Lambda) \lambda_{\min}(\mathbf{Q})}}
\end{aligned} \tag{13}$$

which indicates that, for all $\gamma > 0$, there exists T_γ such that

$$\sqrt{V(\eta(t))} - \frac{\epsilon \beta \lambda_{\max}(\Lambda)}{\sqrt{\lambda_{\min}(\Lambda) \lambda_{\min}(\mathbf{Q})}} \leq \gamma, \quad \forall t \geq T_\gamma. \tag{14}$$

Therefore, we have

$$\|\eta\| \leq \frac{\epsilon \beta \lambda_{\max}(\Lambda)}{\lambda_{\min}(\Lambda) \lambda_{\min}(\mathbf{Q})} + \frac{\gamma}{\sqrt{\lambda_{\min}(\Lambda)}} \leq \nu, \quad \forall t \geq T_\gamma, \tag{15}$$

where the bound $\nu = (\epsilon \beta \lambda_{\max}(\Lambda)) / (\lambda_{\min}(\Lambda) \lambda_{\min}(\mathbf{Q})) + \gamma / \sqrt{\lambda_{\min}(\Lambda)}$. Recalling the scaled estimation error (4), one has

$$\left| \tilde{x}_i \right| \leq \nu \epsilon^{3-i}, \quad \forall t \geq T_\gamma, \quad i = 1, 2, 3, \tag{16}$$

which completes the proof. \square

Remark 1. The observer gain vector \mathbf{L} should be carefully chosen such that the matrix \mathbf{A}_0 is Hurwitz. The method proposed in (Gao 2003; Miklošovic et al. 2006) offers an easy way to design the three elements of \mathbf{L} , in which each parameter is scaled by the LESO bandwidth ω_o using the pole placement approach according to the characteristic equation, that is

$$\begin{aligned}
\lambda(s) &= |s\mathbf{I} - \mathbf{A}_0| = (s + \omega_o)^3, \\
\mathbf{L} &= [3\omega_o, 3\omega_o^2, \omega_o^3]^T.
\end{aligned} \tag{17}$$

Design of ADRC controller

The lumped disturbance has been observed by the ESO. Then, the control law of ADRC is given by

$$u = \frac{u_0 - \hat{x}_3}{b_0}, \tag{18}$$

where b_0 is the estimation of the unknown gain b . Using equation (6) and (17), $h(t)$ can be approximated by $\hat{x}_3(t)$, and the system (2) can be written as

$$\ddot{y} = \frac{b}{b_0} (u_0 - \hat{x}_3) + x_3 \approx u_0. \tag{19}$$

This is reminiscent to the linearization method, where PD control law can be applied to the system (19) to achieve zero steady-state error

$$u_0 = k_p (x_r(t) - \hat{x}_1) + k_d (\dot{x}_r(t) - \dot{\hat{x}}_2), \tag{20}$$

where $x_r(t)$ is the desired trajectory. The parameters of PD control law are selected as $k_p = \omega_c^2$, $k_d = 2\omega_c$, and ω_c denotes the closed-loop bandwidth.

Remark 2. Traditionally, the ADRC control law (20) requires that the lumped disturbance $h(t)$ is precisely estimated by the ESO. However, due to the dramatic variation of rate-dependence hysteresis loop as shown in Figure 1, it cannot be estimated precisely in practice, and this imposes extra restrictions for the usage of ADRC in piezoelectric positioning stages. On the other hand, if we write (19) into

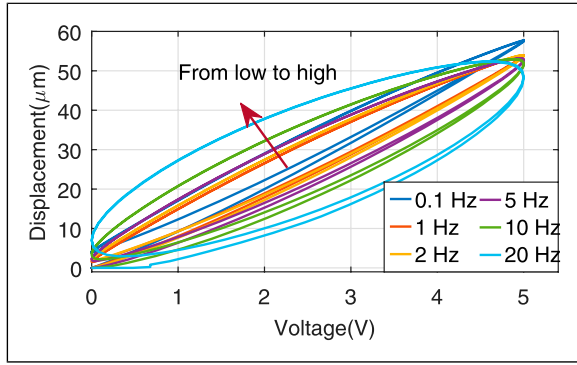


Figure 1. Experiments results of the displacement-voltage hysteresis loops with different rates of input signal.

$$\ddot{y} = \frac{b}{b_0}u_0 + x_3 - \frac{b}{b_0}\hat{x}_3, \quad (21)$$

where b/b_0 is unknown. Hence, the term $x_3 - (b/b_0)\hat{x}_3$ cannot be wiped off by the ESO.

Design of SMCDR controller

As discussed above, the conventional ADRC cannot estimate the lumped disturbance for a piezoelectric nanopositioning system precisely due to the dramatic hysteresis variation. To deal with this problem, a compound controller integrated ADRC and SMC is proposed in this section to address the residual estimation error $\tilde{h}(t)$ and the variation of gain b_0 . The block diagram of the proposed SMCDR controller is shown in Figure 2

$$e_1(t) = x_1(t) - x_r(t), \quad e_2(t) = x_2(t) - \dot{x}_r(t), \quad (22)$$

where $x_1(t)$ is the measured position, $x(t)$ is the velocity, and $x_r(t)$ is the desired trajectory. Then, the tracking error dynamics are given by

$$\dot{e}_1(t) = e_2(t), \quad \dot{e}_2(t) = x_2(t) - \dot{x}_r(t), \quad (23)$$

We define the integral sliding surface as

$$\sigma = e_2(t) + c_1 e_1(t) + c_2 \int_0^t e_1(\tau) d\tau, \quad (24)$$

where c_1 and c_2 are positive control gains. We have the following result.

Theorem 2. Consider system (1) under the control input

$$u = \frac{1}{b_0} \left(u_0 - \hat{x}_3 + u_n \right) \quad (25)$$

$$u_n = -k \text{sign}(\sigma)$$

with parameters satisfying

$$k \geq \left| u_0 - \hat{x}_3 \right| + \mu F + \mu \left| \hat{x}_3 + \Phi \right|, \quad (26)$$

$$\Phi = c_1(x_2 - \dot{x}_r) + c_2(x_1 - x_r) - \ddot{x}_r,$$

where $\mu = \sqrt{b_M/b_m}$; $b_0 = \sqrt{b_M b_m}$; b_M and b_m are the upper and lower bounds of the input gain b , respectively, that is, $b_m \leq b \leq b_M$. Then, the position tracking error $e_1(t)$ defined in equation (22) converges to zero exponentially.

Proof. Substituting the control law equation (25) into (2), yields

$$\dot{x}_2 = \frac{b}{b_0} (u_0 - k \text{sign}(\sigma)) + \left(x_3 - \frac{b}{b_0} \hat{x}_3 \right). \quad (27)$$

The time derivative of sliding variable σ is given by

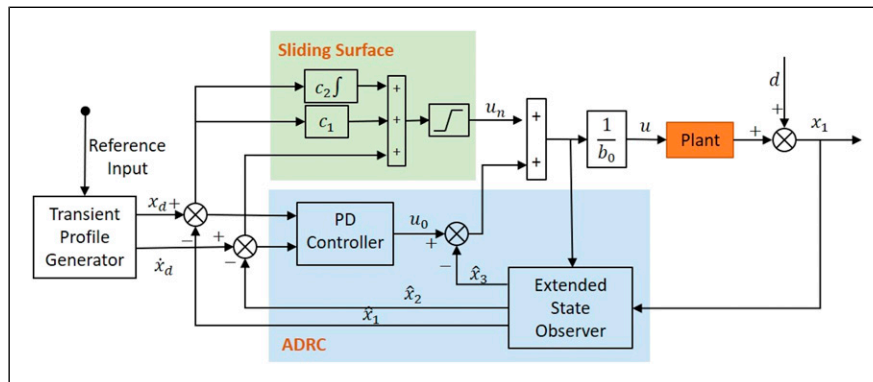


Figure 2. Block diagram of the SMCDR controller.

$$\begin{aligned}
\dot{\sigma} &= \dot{e}_2 + c_1 e_2 + c_2 e_1 \\
&= \dot{x}_2 - \ddot{x}_r + c_1 (x_2 - \dot{x}_r) + c_2 (x_1 - x_r) \\
&= \frac{b}{b_0} (u_0 - k \text{sign}(\sigma)) + \left(x_3 - \frac{b}{b_0} \hat{x}_3 \right) \\
&\quad + \underbrace{c_1 (x_2 - \dot{x}_r) + c_2 (x_1 - x_r) - \ddot{x}_r}_{\Phi}
\end{aligned} \quad (28)$$

Consider the Lyapunov candidate function $V(\sigma) = \frac{1}{2}\sigma^2$, and taking time derivative of $V(\sigma)$, yields

$$\dot{V}(\sigma) = \sigma \dot{\sigma}, \quad (29)$$

To guarantee the finite-time convergence of the sliding variable σ to the origin, the condition $\dot{V}(\sigma) < -\kappa|\sigma|$ should be guaranteed for $\kappa > 0$ along trajectories of the closed-loop system. If the parameter k is selected such that

$$k > \left| \frac{b}{b_0} (x_3 + \Phi) + u_0 - \hat{x}_3 \right|, \quad (30)$$

then using equation (28), we have

$$\begin{cases} \frac{b}{b_0} (u_0 - k \text{sign}(\sigma)) + \left(x_3 - \frac{b}{b_0} \hat{x}_3 \right) + \Phi < -\kappa, & \sigma > 0 \\ \frac{b}{b_0} (u_0 - k \text{sign}(\sigma)) + \left(x_3 - \frac{b}{b_0} \hat{x}_3 \right) + \Phi > \kappa, & \sigma < 0 \end{cases} \quad (31)$$

where $\kappa = k - \sup_{t \geq 0} \{ |b(x_3 + \Phi)/b_0 + u_0 - \hat{x}_3| \}$. Substituting into equation (29), we obtain $\dot{V}(\sigma) < -\kappa|\sigma|$, which implies that $\sigma(t) \rightarrow 0$ in finite time.

Note that

$$\begin{aligned}
\left| \frac{b}{b_0} (x_3 + \Phi) + u_0 - \hat{x}_3 \right| &\leq |u_0 - \hat{x}_3| + \frac{b_0}{b} |x_3 + \Phi|, \\
&\leq |u_0 - \hat{x}_3| + \mu |\tilde{x}_3| + \mu |\hat{x}_3 + \Phi|,
\end{aligned} \quad (32)$$

According to Theorem 1, $|\tilde{x}_3| \leq F$. Thus, the condition $\dot{V}(\sigma) < -\kappa|\sigma|$ is satisfied when k is designed as

$$k \geq |u_0 - \hat{x}_3| + \mu F + \mu |\hat{x}_3 + \Phi|. \quad (33)$$

Finally, on the sliding manifold $\{\sigma = 0\}$, it follows from equation (24) that $|e_1(t), e_2(t)| \rightarrow 0$ exponentially as $t \rightarrow +\infty$, which completes the proof.

Experimental setup and implementation

Experimental setup

The experimental setup is shown in Figure 3 and 4. A flexure-based piezoelectric nanopositioning stage (PI P-603.3S2), which includes strain gauge sensor and piezoelectric actuator, is adopted to evaluate the performance of the proposed control method. The experimental platform can provide the displacement of 380 μm with the excitation voltage ranging from -20 V to +120 V. A real-time controller (Speedgoat real-time target machine) with the data acquiring board (Speedgoat IO133) is used for implementing the controller algorithm. The displacement of the nanopositioning stage is given by the integrated strain gauge sensor through signal conditioner (PI E-509.S3). In addition, a voltage amplifier (PI E-505.00S) with a conversion constant of 10 is used for driving the piezoelectric actuator by amplifying the control voltage.

Transient profile generator

To alleviate the overshoot of setpoint motion tracking while keeping prompt convergence speed, a transient profile with smooth differential value is constructed. The transient profile of target position v expressed in the discrete time optimal solution is given by (Han 2009)

$$\begin{cases} v_1 = v_1 + hv_2, \\ v_2 = v_2 + hu, \quad |u| \leq r, \end{cases} \quad (34)$$

with $u = f_h(v_1 - v, v_2, r_0, h_0)$ and

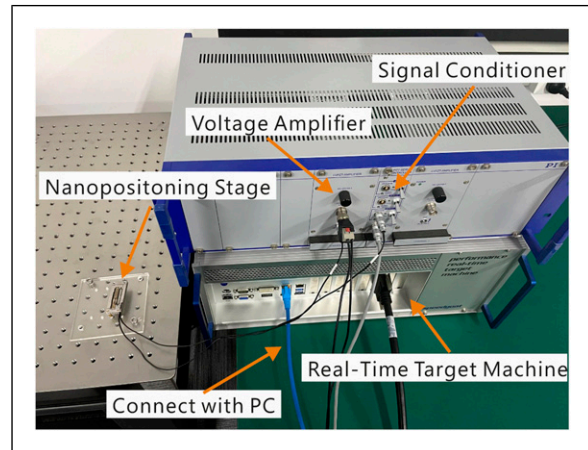


Figure 3. Experimental setup of a piezoelectric nanopositioning stage.

$$\begin{cases} f_h = -r_0(a/d - \text{sign}(a))s_a - r_0\text{sign}(a), \\ d = h_0^2 r_0, a_0 = h_0 v_2, y = v_1 + a_0, \\ a_1 = \sqrt{d(d + 8|y|)}, \\ a_2 = a_0 + \text{sign}(y)(a_1 - d)/2, \\ s_y = (\text{sign}(y + d) - \text{sign}(y - d))/2, \\ a = (a_0 + y - a_2)s_y + a_2, \\ s_a = (\text{sign}(a + d) - \text{sign}(a - d))/2, \end{cases} \quad (35)$$

where v_1 is the constructed transient trajectory with velocity v_2 , the maximum response speed of the physical device is limited by desired speed r . Parameters r_0 and h_0 are to be designed in accordance with the physical device, which are set to r and h , respectively.

Implementation of ESO

The ESO model in equation (2) is discretized with zero-order-hold (ZOH) method to facilitate the implementation in physical device

$$\begin{aligned} \hat{\mathbf{X}}_{k+1} &= \Phi \hat{\mathbf{X}}_k + \Gamma u_k, \\ \hat{y}_k &= \mathbf{H} \hat{\mathbf{X}}_k + \mathbf{J} u_k, \end{aligned} \quad (36)$$

where

$$\Phi = e^{AT} = \begin{bmatrix} 1 & T & \frac{T^2}{2} \\ 0 & 1 & T \\ 0 & 0 & 1 \end{bmatrix}$$

$$\Gamma = \int_0^T e^{A\tau} d\tau \mathbf{B} = \begin{bmatrix} b \frac{T^2}{2} \\ bT \\ 0 \end{bmatrix}$$

$$\mathbf{H} = [1 \quad 0 \quad 0], \mathbf{J} = [0]$$

and T is the sampling time. The discrete form of ESO (Li et al. 2012) is given by

$$\begin{aligned} \hat{\mathbf{X}}_{k+1} &= \Phi \hat{\mathbf{X}}_k + \Gamma u_k + \Phi \mathbf{L}_d (y_k - \hat{y}_k), \\ \hat{y}_k &= \mathbf{H} \hat{\mathbf{X}}_k + \mathbf{J} u_k. \end{aligned} \quad (37)$$

To simplify the parameter tuning, as shown in Remark 1, each observer parameter is scaled by the observer bandwidth ω_o using the pole placement of the characteristic equation, which gives

$$\lambda(s) = |z\mathbf{I} - (\Phi - \Phi \mathbf{L}_d \mathbf{H})| = (z - \beta)^3, \quad (38)$$

where the pole of discrete ESO $\beta = e^{-\omega_o T}$. Finally, the parameters of discrete ESO are chosen as

$$\mathbf{L}_d = \begin{bmatrix} 1 - \beta^3 \\ (1 - \beta)^2 (1 + \beta) \frac{3}{2T} \\ (1 + \beta)^3 \frac{1}{T^2} \end{bmatrix}. \quad (39)$$

Parameters of SMCDR

To implement ADRC method, the minimal model information is needed, for example, the order of the dynamic model. The second-order transfer function of the nano-positioning stage is identified as

$$\mathbf{G}(s) = \frac{1.255 \times 10^7}{s^2 + 2372s + 3.2 \times 10^6}. \quad (40)$$

Therefore, b_0 can be selected as 1.255×10^7 for this stage. The experimental plant has a natural frequency of 284 Hz. The desired controller bandwidth is chosen as $\omega_c = 150$ Hz. The desired observer bandwidth ω_o should be chosen between $3 \omega_c$ to $5 \omega_c$, and, 450 Hz is selected. The sampling time is $T = 0.0001$ s, and the parameters of the proposed SMCDR controller are chosen as follows: $k = f \times 10^5$ (f is the frequency of reference signal), $c_1 = 16$, $c_2 = 8$, and $\phi = 10$. The parameters of transient profile generator r_0 and h_0 are selected as 2×10^4 and 10^{-4} , respectively. A PID controller tuned by MATLAB PID autotuner with parameters $K_p = 0.0842$, $K_i = 39.4$, $K_d = 7 \times 10^{-5}$, and filter coefficient $N = 100$ is also applied to comparison study.

Remark 3. The signum function in control law equation (25) is substituted with the following saturation function to relieve chattering phenomenon

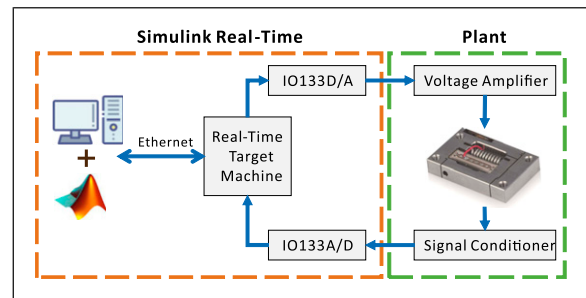


Figure 4. Block diagram of experimental setup.

$$\text{sat}(\sigma/\phi) = \begin{cases} \text{sign}(\sigma), & \text{if } |\sigma| > \phi, \\ \sigma/\phi, & \text{if } |\sigma| \leq \phi, \end{cases} \quad (41)$$

where ϕ is the thickness of boundary layer. A large boundary ϕ is selected to suppress the chattering problem in experiments, which would deteriorate the performance of the proposed controller.

Remark 4. In practice, the achievable controller bandwidth is limited not only by the physical system but also by the presence of sensor noises and dynamics uncertainties. Note that the controller bandwidth ω_c is also a trade-off between control performance and closed-loop stability. The lower the bandwidth ω_c , the worse the tracking performance. In this work, we select ω_c using the method presented in Sect. 3.4 of (Gao 2003). That is, we first select an initial value, and then increase ω_c until that the control signals becomes excessively noisy or there exist oscillatory behaviors.

Experimental results

To verify the efficiency of the proposed controller, motion tracking and regulation experiments are carried out with sinusoidal, triangular and pseudo-step trajectories, respectively. In addition, external disturbances are introduced to validate the robustness of SMCDR. For comparison study, the conventional ADRC, the integral sliding mode control (ISMC) and PID controllers are implemented to generate their best results.

Sinusoidal trajectory tracking results

To evaluate the effectiveness and accuracy of the proposed SMCDR for the particular application, 20 μm peak-to-peak sinusoidal trajectories with various frequencies are adopted for trajectory tracking.

The experimental results of trajectory tracking for 10 Hz sine wave are shown in Figure 5. It can be seen from

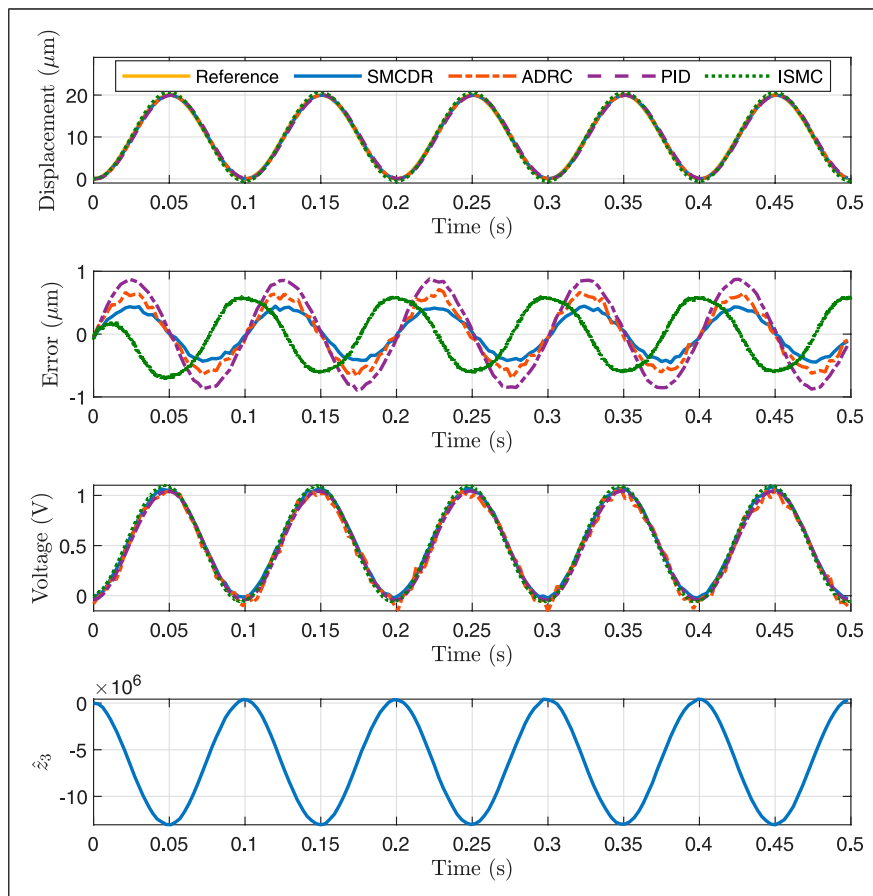


Figure 5. Trajectory tracking results of sine wave with 10-Hz frequency. (a) The displacement trajectory, (b) position tracking errors, (c) control signals, and (d) estimated disturbance \hat{z}_3 .

Figure 5 that the proposed SMCDR has the trajectory with high precision. The maximum position tracking error of SMCDR is limited in $0.45\mu\text{m}$, that is, 2.25% of the motion range, which is significantly reduced comparing with ISMC, ADRC, and PID controllers. In particular, the ISMC produces the MAXE (maximum error) of 3.11% of the motion range; the conventional ADRC produces the MAXE of 3.69% of the motion range; and the PID controller produces the MAXE of 4.50% of the motion range.

The experimental results of 50 Hz sine wave tracking are shown in Figure 6. It can be observed that the proposed SMCDR controller generates the RMSE (root mean square error) and MAXE relative errors of 2.98% and 4.53%, respectively. Although the ISMC produces the RMSE of 3.16% and MAXE of 6.79%, the conventional ADRC produces the RMSE of 11.65% and MAXE of 16.99%. In addition, the RMSE and MAXE of 13.51% and 19.66%, respectively, are obtained by the PID controller.

Moreover, the comparisons of position tracking errors with different input frequencies are shown in Table 1. It can be seen that the RMSEs of SMCDR controller are 37.90%, 29.77%, 60.06%, and 5.70% lower than those of ISMC,

30%, 30.73%, 69%, and 74.44% lower than those of ADRC, and 49.67%, 50.33%, 77.01%, and 77.94% lower than those of PID method under 5, 10, 20, and 50 Hz input frequencies, respectively. Hence, it demonstrates that the SMCDR has an obvious performance improvement with the increasing of input frequencies, while keeping a concise controller architecture.

The triangular waves are widely used in piezoelectric nanopositioning applications, 20 μm peak-to-peak triangular trajectories with various frequencies are applied to evaluate tracking performance of the proposed method.

It can be observed that the presented SMCDR has high precision, and the maximum position tracking error of SMCDR is limited in $0.32\mu\text{m}$, that is, 1.61% of the motion range, which has an obvious tracking accuracy compared with ISMC, ADRC, and PID controllers. In particular, the ISMC produces the MAXE of 4.36% of the motion range, the conventional ADRC produces the MAXE of 3.20% of the motion range, and the PID controller produces the MAXE of 4.40% of the motion range, as shown in Figure 7. Similar results of 50 Hz triangular wave tracking can also be made as displayed in Figure 8. The detailed comparison of

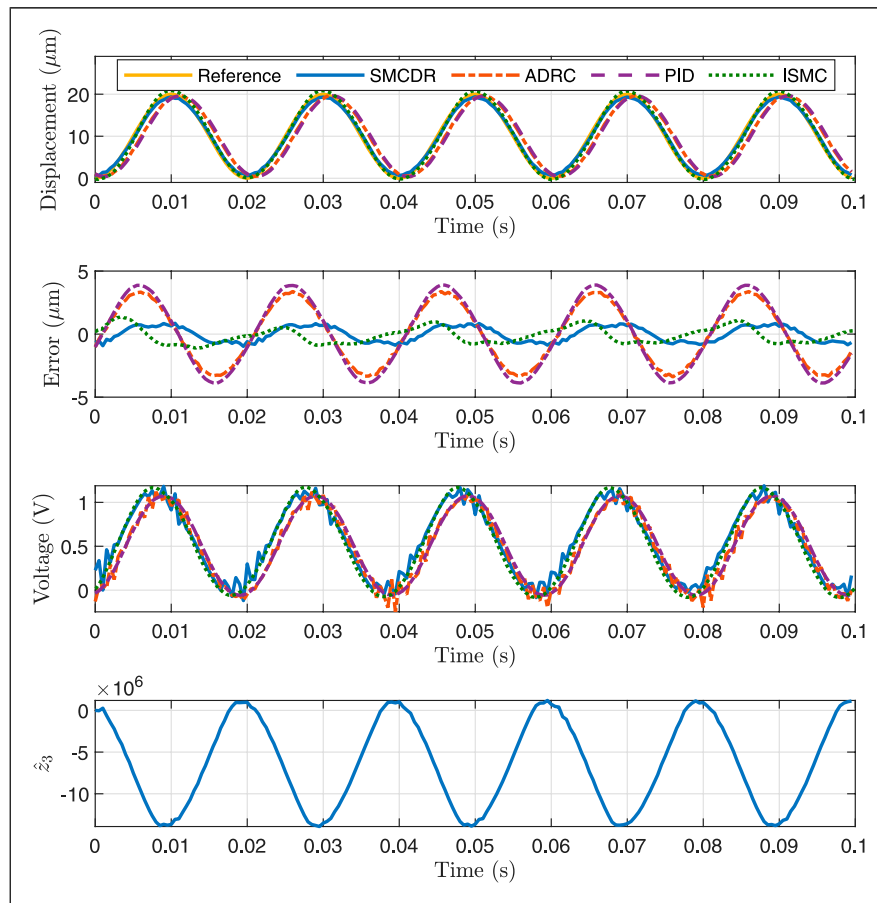


Figure 6. Trajectory tracking results of sine wave with 50-Hz frequency. (a) The displacement trajectory, (b) position tracking errors, (c) control signals, (d) estimated disturbance \hat{z}_3 .

Table 1. Experimental results of sinusoidal trajectory tracking.

Signal	Error	PID (%)	ADRC (%)	ISMIC (%)	SMCDR (%)
5 Hz	RMSE	1.53	1.10	1.24	0.77
Sine wave	MAXE	2.33	2.14	1.95	1.36
10 Hz	RMSE	3.04	2.18	2.15	1.51
Sine wave	MAXE	4.50	3.69	3.11	2.25
20 Hz	RMSE	5.96	4.42	3.43	1.37
Sine wave	MAXE	8.67	6.84	5.06	2.52
50 Hz	RMSE	13.51	11.66	3.16	2.98
Sine wave	MAXE	19.66	16.99	6.79	4.53

Triangular trajectory tracking results.

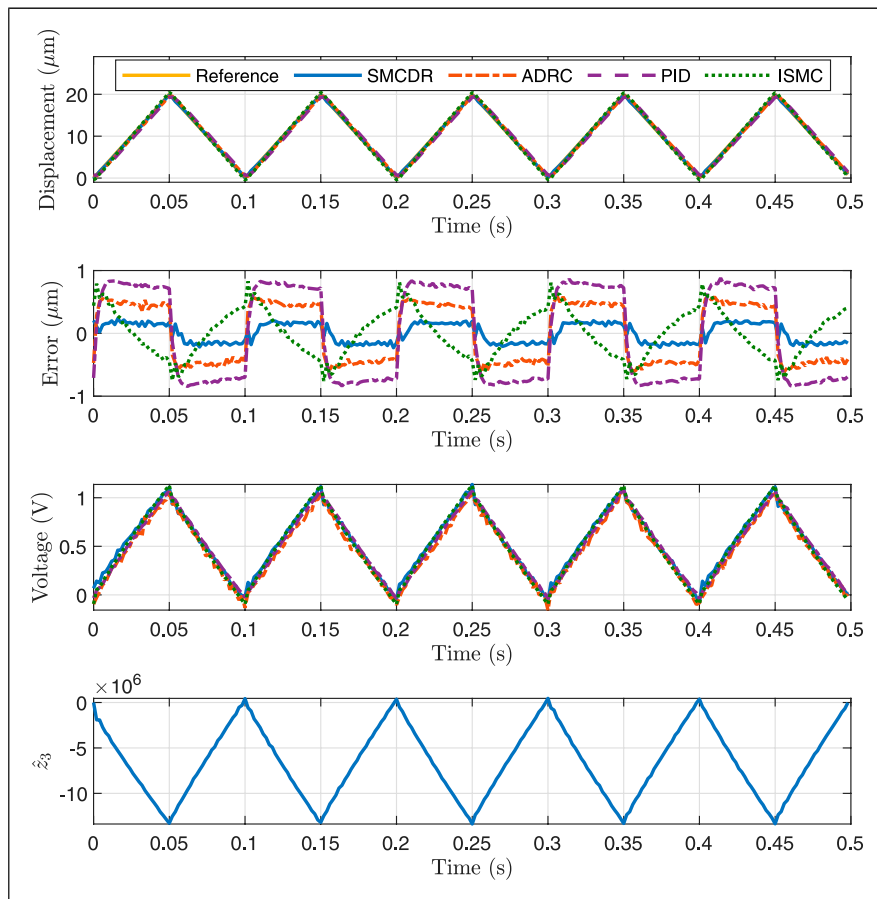


Figure 7. Trajectory tracking results of triangular wave with 10-Hz frequency. (a) The displacement trajectory, (b) position tracking errors, (c) control signals and (d) estimated disturbance \hat{z}_3 .

triangular waves tracking performance under different input frequencies can be found in Table 2.

Remark 5. The switching gain k of SMCDR is determined by \ddot{x}_r as shown in (26). Theoretically, the acceleration of triangular trajectories is unbounded at the turning points. In practice, it can hardly generate a sharp signal such that the acceleration is unbounded due to the physical limitations. Therefore, it is reasonable to bound the reference

acceleration signals in a bounded interval. The range of \ddot{x}_r of triangular waves is saturated in $[-10^4, 10^4]$ during the controller implementation.

Step position tracking results

The step trajectory is chosen as a reference signal since reaching the desired position is a common scenario for the nanopositioning stage during object operations, such as

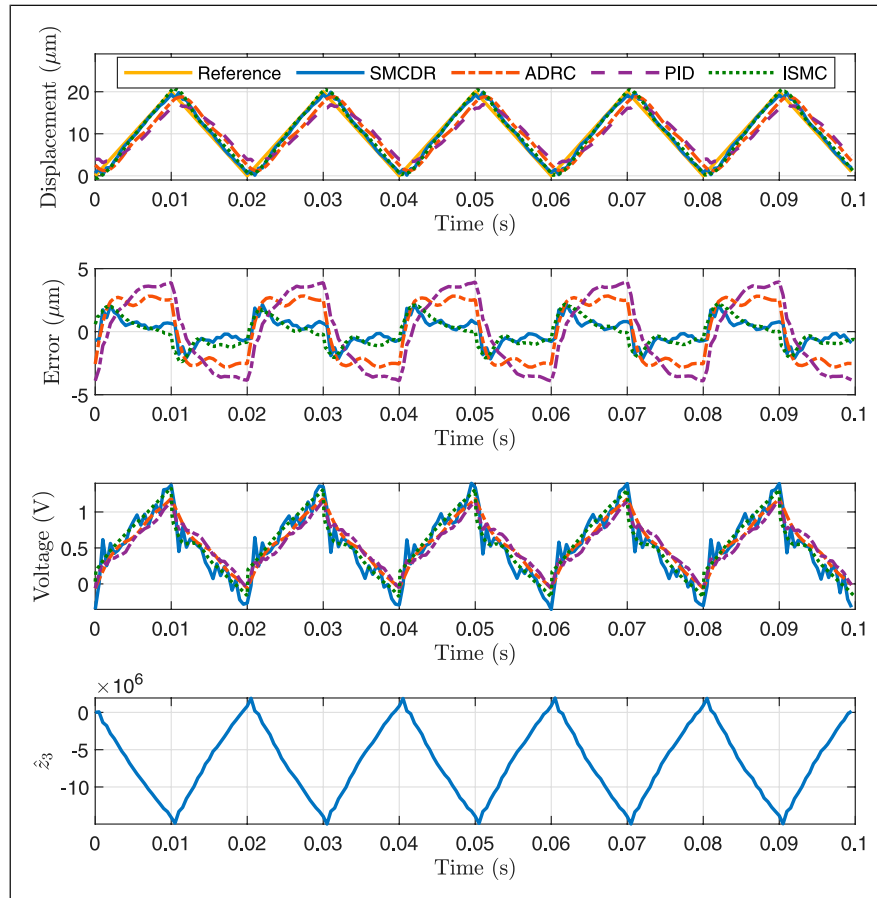


Figure 8. Trajectory tracking results of Triangular wave with 50-Hz frequency. (a) The displacement trajectory, (b) position tracking errors, (c) control signals, and (d) estimated disturbance \hat{z}_3 .

Table 2. Experimental results of triangular trajectory tracking.

Signal	Error (%)	PID (%)	ADRC (%)	ISMC (%)	SMCDR (%)
5 Hz	RMSE	1.88	1.37	1.10	0.87
Triangular wave	MAXE	2.44	1.76	2.61	1.30
10 Hz	RMSE	3.68	2.37	1.88	0.77
Triangular wave	MAXE	4.40	3.20	4.36	1.61
20 Hz	RMSE	7.00	5.21	2.88	1.18
Triangular wave	MAXE	8.24	5.97	6.43	3.20
50 Hz	RMSE	14.38	11.80	5.54	4.65
Triangular wave	MAXE	19.72	14.34	11.23	10.88

gripping and cell injecting. However, a trade-off between the response overshoot and speed is inevitable for the controller design.

To mitigate this situation, the pseudo step signal is generated by transient profile generator. The tracking results of pseudo step signal with magnitude of 10 μm are given in Figure 9. It can be seen that all controllers achieve fast response with small overshoot for the target position. Sliding mode control integrated with active disturbance rejection has the best performance with 1.22% overshoot,

which is 21.21%, 61.39%, and 71.63% lower than those of ISMC, ADRC, and PID controllers, respectively.

Disturbance rejection results

To verify the disturbance rejection performance of the proposed SMCDR, a short external disturbance clip is manually introduced after the step response. The following external disturbance with hybrid frequencies is injected

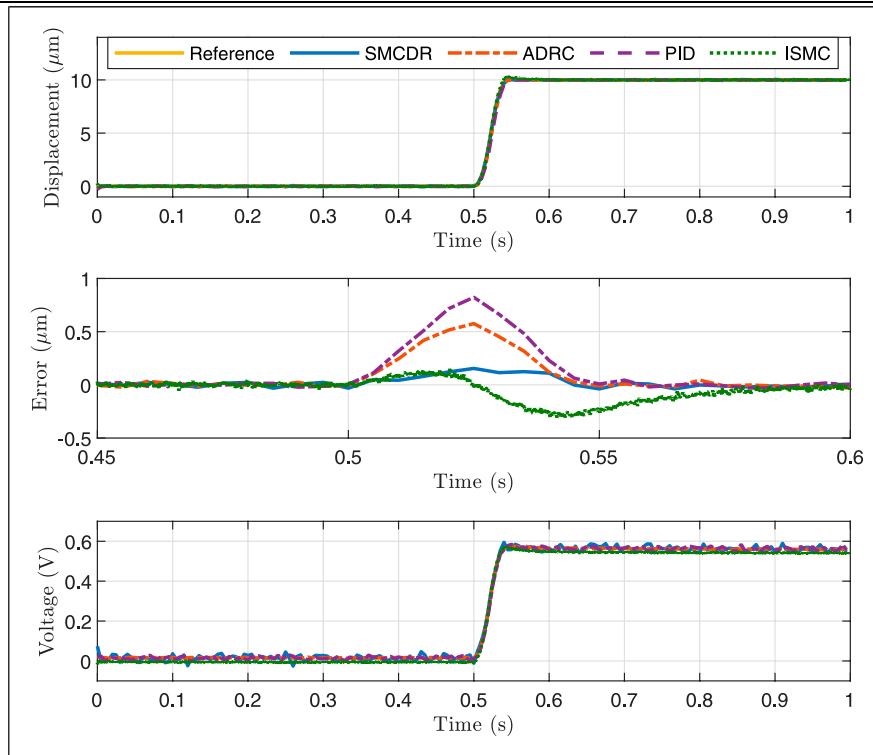


Figure 9. Trajectory tracking results of pseudo step signal with 10- μm amplitude. (a) The desired trajectory, (b) position tracking errors, and (c) control signals.

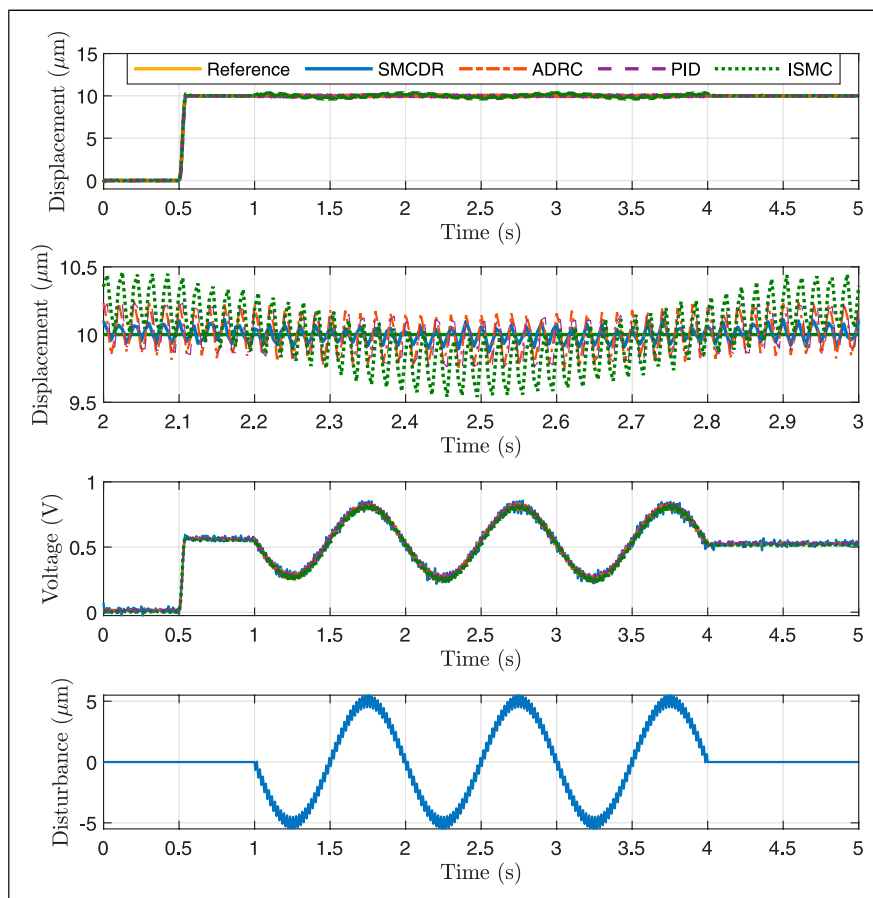


Figure 10. Experimental results of disturbance rejection. (a) The displacement trajectory, (b) position tracking errors, (c) control signals, and (d) the external disturbance $d(t)$.

$$d(t) = [0.5 \sin(100\pi t) + 5 \sin(2\pi t)] \mu\text{m}.$$

The experimental results in Figure 10 indicate that the proposed SMCDR controller exhibits an outstanding ability for attenuating disturbance with different frequencies. It can be seen that SMCDR created the control performance with RMSE and MAXE disturbance rejection errors of 0.0542 μm and 0.2434 μm , respectively, which demonstrates a better performance for hybrid frequencies disturbance compared with ADRC and PID controller.

The foregoing experimental results indicate that the proposed SMCDR achieved a satisfying position tracking accuracy while keeping a simple architecture. Compared to the existing controllers, the proposed SMCDR controller has higher accuracy with a tracking error of 0.17% lower for 5 Hz sine wave trajectory tracking, which is better than the RMSE of 2.15% obtained by a discrete sliding mode controller (Xu 2014) and that achieved by an output feedback sliding-mode controller (Xu and Tan 2016). Moreover, it also obtained a better performance than the feedforward controller with inverse hysteresis model as reported in (Ang et al. 2007) for sinusoidal trajectory tracking.

Conclusion

In this work, a novel SMCDR controller has been proposed for precise trajectory tracking of a piezoelectric nanopositioning stage. The proposed controller combines the strength of both SMC and ADRC. The ADRC is used to estimate the lumped disturbance, while the SMC is adopted to compensate for the estimation error and model uncertainties. The superiority of the proposed SMCDR is that it does not require the knowledge of system parameters except for a rough control gain, which eliminates the dependence on complicated mathematical models and state observers. The exponential stability of the SMCDR strategy has been proved based on Lyapunov's direct method, and its effectiveness has been demonstrated by conducting a series of experimental studies. As compared with PID, ISMC, and ADRC controllers, the proposed SMCDR control has shown higher tracking accuracy and better disturbance rejection ability while maintaining a simple controller structure, which facilitates practical implementation. The higher-order sliding mode controller is expected to be integrated to overcome chattering problem in the future work.

Declaration of conflicting interests

The author(s) declared no potential conflicts of interest with respect to the research, authorship, and/or publication of this article.

Funding

This work was supported in part by the Science and Technology Foundation of Guizhou Province under Grant [2020]1Y233, the

Innovation and Entrepreneurial Project of Guizhou Province for High-level Overseas Talents under Grant (2020)04, the Foundation of Guizhou University under Grant [2020]51, (2019)67, and GZUAMT2021KF[03].

References

- Alonge F, Cirrincione M, D'Ippolito F, et al. (2017) Robust active disturbance rejection control of induction motor systems based on additional sliding mode component. *IEEE Transactions on Industrial Electronics* 64(7): 5608–5621.
- Ang WT, Khosla PK and Riviere CN (2007) Feedforward controller with inverse rate-dependent model for piezoelectric actuators in trajectory-tracking applications. *IEEE/ASME Transactions on Mechatronics* 12(2): 134–142.
- Feng Z, Ling J, Ming M, et al. (2019) Integrated modified repetitive control with disturbance observer of piezoelectric nanopositioning stages for high-speed and precision motion. *Journal of Dynamic Systems, Measurement, and Control* 141(8).
- Gao Z (2003) Scaling and bandwidth-parameterization based controller tuning. In: *Proceedings of the American control conference*, 6. pp. 4989–4996.
- Gu GY, Zhu LM, Su CY, et al. (2014) Modeling and control of piezo-actuated nanopositioning stages: A survey. *IEEE Transactions on Automation Science and Engineering* 13(1): 313–332.
- Guo BZ and Zhao ZL (2011) On the convergence of an extended state observer for nonlinear systems with uncertainty. *Systems & Control Letters* 60(6): 420–430.
- Han J (1998) Active disturbance rejection control and its application. *Control and Decision* 13(1): 19–23.
- Han J (2009) From PID to active disturbance rejection control. *IEEE Transactions on Industrial Electronics* 56(3): 900–906.
- Lau JY, Liang W and Tan KK (2019) Motion control for piezoelectric-actuator-based surgical device using neural network and extended state observer. *IEEE Transactions on Industrial Electronics* 67(1): 402–412.
- Li C, Yang H, Jenkins LL, et al. (2015a) Enhanced-performance control of an electromagnetic solenoid system using a digital controller. *IEEE Transactions on Control Systems Technology* 24(5): 1805–1811.
- Li CX, Ding Y, Gu GY and Zhu LM (2016) Damping control of piezo-actuated nanopositioning stages with recursive delayed position feedback. *IEEE/ASME Transactions on Mechatronics* 22(2): 855–864.
- Li D, Yang H, Qi N and Yuan J (2021) Observer-based sliding mode control for piezoelectric wing bending-torsion coupling flutter involving delayed output. *Journal of Vibration and Control* 27(15–16): 1824–1841.
- Li L, Chen Z, Aphale SS and Zhu L (2020) Fractional repetitive control of nanopositioning stages for high-speed scanning using low-pass fir variable fractional delay filter. *IEEE/ASME Transactions on Mechatronics* 25(2): 547–557.
- Li P, Li P and Sui Y (2015b) Adaptive fuzzy hysteresis internal model tracking control of piezoelectric actuators with nanoscale application. *IEEE Transactions on Fuzzy Systems* 24(5): 1246–1254.
- Li S, Yang J, Chen WH and Chen X (2012) Generalized extended state observer based control for systems with mismatched

- uncertainties. *IEEE Transactions on Industrial Electronics* 59(12): 4792–4802.
- Ling J, Feng Z, Kang X and Xiao X (2021) Bandwidth enhancement in damping control for piezoelectric nanopositioning stages with load uncertainty: Design and implementation. *Journal of Vibration and Control* 27(11–12): 1382–1394.
- Miklošovic R, Radke A and Gao Z (2006) Discrete implementation and generalization of the extended state observer. In: *Proceedings of 2006 American Control Conference*. New York, NY: IEEE, pp. 2209–2214.
- Nguyen ML and Chen X (2019) Mpc inspired dynamical output feedback and adaptive feedforward control applied to piezo-actuated positioning systems. *IEEE Transactions on Industrial Electronics* 67(5): 3921–3931.
- Ovalle L, Rios H, Llama M and Fridman L (2021) Continuous sliding-mode output-feedback control for stabilization of a class of underactuated systems. *IEEE Transactions on Automatic Control* .67, 986–992,
- Ramírez-Neria M, Morales-Valdez J and Yu W (2021) Active vibration control of building structure using active disturbance rejection control. *Journal of Vibration and Control*: 1–6.
- Sabarianand D, Karthikeyan P and Muthuramalingam T (2020) A review on control strategies for compensation of hysteresis and creep on piezoelectric actuators based micro systems. *Mechanical Systems and Signal Processing* 140: 106634.
- Shahabi P, Ghafarirad H and Taghvaeipour A (2020) High-frequency robust position control of a nonlinear piezoelectric bending actuator. *Journal of Vibration and Control* 26(17–18): 1560–1573.
- Tao Y, Li L, Li HX and Zhu L (2021) High-bandwidth tracking control of piezoactuated nanopositioning stages via active modal control. *IEEE Transactions on Automation Science and Engineering*: 1–9.
- Utkin V, Guldner J and Shi J (2017) *Sliding mode control in electro-mechanical systems*. Boca Raton, Florida: CRC press.
- Wang G and Xu Q (2017) Design and precision position/force control of a piezo-driven microinjection system. *IEEE/ASME Transactions on Mechatronics* 22(4): 1744–1754.
- Wang G and Xu Q (2018) Adaptive terminal sliding mode control for motion tracking of a micropositioning system. *Asian Journal of Control* 20(3): 1241–1252.
- Wu Y, Yu X and Man Z (1998) Terminal sliding mode control design for uncertain dynamic systems. *Systems & Control Letters* 34(5): 281–287.
- Xia Y, Fu M, Li C, et al. (2018) Active disturbance rejection control for active suspension system of tracked vehicles with gun. *IEEE Transactions on Industrial Electronics* 65(5): 4051–4060.
- Xie H, Wen Y, Shen X, et al. (2019) High-speed afm imaging of nanopositioning stages using h_∞ and iterative learning control. *IEEE Transactions on Industrial Electronics* 67(3): 2430–2439.
- Xu Q (2014) Discrete-time second-order sliding mode control for a nanopositioning stage. In: *Proceedings of the 33rd Chinese Control Conference*. New York, NY: IEEE, pp. 7976–7981.
- Xu Q and Tan KK (2016) Digital sliding-mode control of high-order systems. In: *Advanced Control of Piezoelectric Micro-/Nano-Positioning Systems*. New York, NY: Springer, pp. 147–165.
- Yang C, Wang Y and Youcef-Toumi K (2020) Feedback-assisted feedforward hysteresis compensation: A unified approach and applications to piezoactuated nanopositioners. *IEEE Transactions on Industrial Electronics* 68(11): 11245–11254.
- Yao S, Gao G and Gao Z (2021) On multi-axis motion synchronization: The cascade control structure and integrated smc–adrc design. *ISA transactions* 109: 259–268.
- Yousef HA, Hamdy M, Saleem A, et al. (2019) Enhanced adaptive control for a benchmark piezoelectric-actuated system via fuzzy approximation. *International Journal of Adaptive Control and Signal Processing* 33(9): 1329–1343.
- Zhang Y, Yan P and Zhang Z (2017) Robust adaptive backstepping control for piezoelectric nano-manipulating systems. *Mechanical Systems and Signal Processing* 83: 130–148.